

# Multiscale Study of Interfacial Intermetallic Compounds in a Dissimilar Al 6082-T6/Cu Friction-Stir Weld

M.N. AVETTAND-FENOËL, R. TAILLARD, G. JI, and D. GORAN

The objective of this work was to characterize the  $Al_xCu_y$  intermetallic compounds (IMCs) formed at the abutting interface during solid-state friction-stir welding (FSW) of 6082 aluminum alloy and pure copper. As IMCs are potential sources of flaws in case of mechanical loading of welds, their study is essential at various scale lengths. In the present case, they have been identified by neutron diffraction, electron backscattered diffraction, and transmission electron microscopy. Neutron diffraction analyses have shown that a shift of the tool from the interface, in particular towards the Cu part, generates an increase of the IMCs' volume fraction. In accordance with an exacerbation of its kinetics of formation by FSW, a 4- $\mu$ m-thick layer has precipitated at the interface despite the shortness of the thermal cycle. This layer is composed of two sublayers with the  $Al_4Cu_9$  and  $Al_2Cu$  stoichiometry, respectively. Convergent beam electron diffraction analyses have, however, disclosed that the crystallography of the current  $Al_2Cu$  compound does not comply with the usual tetragonal symmetry of this phase. The  $Al_2Cu$  phase formation results from both the local chemical composition and thermodynamics, whereas the development of  $Al_4Cu_9$  is rather due to both the local chemical composition and the shortness of the local FSW thermal cycle.

DOI: 10.1007/s11661-012-1277-3

© The Minerals, Metals & Materials Society and ASM International 2012

## I. INTRODUCTION

FRICION-STIR welding (FSW) is a solid-state bonding technique first developed for welding of Al alloys (such as 2xxx and 7xxx), which are difficult to fusion weld without hot cracking, porosity, or distortion.<sup>[1-3]</sup> As FSW operates in the solid state, it was naturally extended to the very strategic challenge of the joining of dissimilar reactive materials<sup>[3,4]</sup> with the aim of reducing the amount of intermetallic compounds (IMCs) by comparison with traditional fusion welding processes. IMCs are readily formed at the faying interface during the welding of metals with high chemical affinity. Due to their inherent brittleness, it is necessary to prevent the extensive formation of continuous IMCs layers along the interface in order to ensure suitable mechanical properties to the joint.<sup>[5-12]</sup> This goal requires a careful study of the IMCs microstructure in order to investigate in detail their mechanism of formation. Such knowledge should be pertinent so as to decrease their kinetics of formation by means of judicious modifications of the processing parameters and/or of the interface chemical composition. More precisely, it is important to underline that a continuous reaction layer with an optimal thickness is most often required in order to obtain sound bonds by diffusion.<sup>[13]</sup>

Whatever the welding process and the chemical nature of the parent alloys, too thick layers of intermetallics are indeed deleterious for the mechanical behavior of the joints.<sup>[11,14-18]</sup> Favorable effects of small changes of the chemical composition of the base materials on the kinetics of formation and nature of the IMCs with profitable consequences for the mechanical behavior of the joints have also been reported.<sup>[19,20]</sup> For instance, in the case of diffusion welding of a Si-bearing Al alloy to a Ti alloy, the presence of a silicon content of 1.2 pct was shown to slow down the Al diffusion towards Ti; Si enabled to master the growth of the diffusion layer at the interface, improving the mechanical properties of the joint.<sup>[20]</sup> Likewise, 1.5 pct Si and 1 pct Cu additions to 6000 Al alloys have been shown to change the nature of IMCs formed at the 6000 Al alloy/steel interface obtained by diffusion welding. Instead of  $Al_3Fe$ , a Cu-rich  $Al_{12}FeSi$  IMC has formed. These modifications of both the nature and the crystal structure of the IMCs in the interfacial layer have led to an increase of the weld ductility, very likely because of a multiplication of slip planes.<sup>[19]</sup> In addition, a sustained attention must be paid to the effects of a change of the mechanism of the chemical reaction by the presence of a coating or of a transition layer with a judicious chemical composition at the faying interface.<sup>[16,17]</sup> For instance, the insertion of a thin foil of zinc at an Al alloy/pure Cu interface would reduce the amount of harmful IMCs formed during FSW, which gives rise to a significant increase of the average fracture load of the joints.<sup>[16]</sup> This result must nevertheless be questioned because of both the rather low melting point of Zn and the high chemical affinity between Cu and Zn that overcomes the Al/Cu one.<sup>[21-24]</sup> In the same way, and concerning this time coated

M.N. AVETTAND-FENOËL, Assistant Professor, R. TAILLARD, Professor, and G. JI, Research Scientist, are with the Unité Matériaux Et Transformations (UMR CNRS 8207), Lille 1 University, 59655 Villeneuve d'Ascq, France. Contact e-mail: marie-noelle.avettand-fenoel@univ-lille1.fr D. GORAN, Scientist, is with the Bruker Nano GmbH, 12489 Berlin, Germany.

Manuscript submitted January 19, 2012.

Article published online June 27, 2012

steel–Al alloy FSW joints, the presence of a Zn-based coating causes the formation of an Al–Zn eutectic film, which removes the oxide film at the Al surface and therefore promotes the dissimilar bonding by means of the formation of Al-rich  $\text{Al}_x\text{Fe}_y$  compounds.<sup>[17]</sup> The nature of the interfacial IMC is further strongly dependent on the thermomechanical aspects of the welding process, that is to say, on the homogeneity and amplitude of the plastic deformation at and close to the interface, as well as on the heating and cooling rates. Such a feature is exacerbated for the FSW case where the distance of atomic diffusion must be changed from place to place because of both the variation between local thermal cycles and the very high heterogeneity of the plastic flow pattern.<sup>[25,26]</sup> Thermal diffusion occurs because a close to 0.8 peak value of homologous temperature is required in order to achieve a suitable material flow.<sup>[3,4]</sup> Mechanical mixing and short-circuit diffusion may also happen as very drastic plastic strains ranging from 2 to approximately 130<sup>[27–32]</sup> are predicted to occur in local areas within the nugget. The effectiveness of such phenomena is the most likely as local and transient high supersaturations of vacancies are generated at high strain rates<sup>[33,34]</sup> and therefore at the 1 to 650  $\text{s}^{-1}$ <sup>[3,4,27,30,32,35–39]</sup> values commonly assessed during FSW. Furthermore, the favorable effect of a discontinuity of IMCs layers on the joint strength has also been reported.<sup>[40]</sup> All of these observations prove the chief interest of a thorough study of the microstructure of the IMCs layers formed in dissimilar welds in order to improve the mechanical resistance of the bond by means of a change of the processing parameters. Heretofore, only few studies have dealt with the fine microstructure of the interfacial area in dissimilar FSW welds, however, made of materials other than Al and Cu alloys.<sup>[41–44]</sup> According to the systems, the interfacial zones were shown to consist either in interdiffusion or in intermetallic areas. By way of examples, i) the presence of an interdiffusion zone extending over a 1.5 to 1.8  $\mu\text{m}$  distance was proved by energy dispersive spectroscopy (EDX)/transmission electron microscopy (TEM) at the interface of Fe–Ni samples<sup>[41]</sup>; ii) electron diffraction analyses put into evidence a 250-nm-thick interfacial layer of  $\text{Al}_4\text{Fe}$  in an Al alloy–austenitic stainless steel joint<sup>[42]</sup>; iii) a 1- $\mu\text{m}$ -thick interface made of intercalated lamellae enriched in Al or Ti–V was observed by EDX/TEM in Al 6061–T6–Ti–6 pct Al–4 pct V friction stir joint<sup>[43]</sup>; iv) the presence of the  $\text{Al}_{12}\text{Mg}_{17}$  IMC in the 1- $\mu\text{m}$ -thick interfacial layer of an AA6040 Al alloy–AZ31 Mg alloy friction-stir weld was further established by electron diffraction.<sup>[44]</sup> For the case of Al–Cu FSW, a rather global characterization of the interface has only been carried out.<sup>[5,45]</sup> X-ray diffractometry combined with selective etching has revealed the presence of two sublayers of  $\text{Al}_2\text{Cu}$  and  $\text{Al}_4\text{Cu}_9$  within a 1- $\mu\text{m}$ -thick continuous and uniform layer at a Al–1060–pure Cu interface.<sup>[5]</sup> For the same system, SEM analyses have also shown that according to the rotational speed, comprised between 400 and 1000 rpm, the thickness of the interface changes from 0.3 to 3  $\mu\text{m}$ , respectively.<sup>[45]</sup> The too macroscopic scale of these investigations justifies the current study of a 6082–T6 Al alloy/Cu–al combination more especially as it is further concerned by

numerous potential uses. Potential applications of such joints will be in the fields of power generation and energy transmission because of both their attractive thermal and electrical conductivities and of significant savings. This article focuses on a multiscale study of interfacial IMCs. The macroscopic investigation was essentially achieved by neutron diffraction, whereas at a finer scale, the study was performed by both electron backscattered diffraction and transmission electron microscopy.

## II. EXPERIMENTAL PROCEDURE

Two 5-mm-thick 6082–T6 aluminum alloy and Cu–al plates were abutted and friction-stir welded perpendicularly to their rolling direction. Joining was conducted under a 1500-kg controlled axial force with a clockwise rotation rate of 800 rpm and at a transverse speed of 750 mm/min. The tool was made of a heat-treated Z38CD5 steel with a hardness of 50 HRC. It comprised a 15-mm-diameter concave shoulder prolonged by a pin. This 4.8-mm long probe was a M4 threaded tapered cylinder with a diameter of 9.7 mm at the root and 3 mm at the edge, respectively. The tool was 2.5 deg backward tilted and located at the faying interface (WI), or at a distance of 1 mm from this interface either in the Cu advancing side (WCu) or in the Al retreating side (WAl). Neutron diffraction experiments were performed in the bulk of the three kinds of seams by using the high-flux multi-detector (800 cells) G4.1 diffractometer at Laboratoire Léon Brillouin in France. A wavelength of 2.423 Å was used for the determination of both the nature and volume fraction of the intermetallic compounds in the welds. The investigations were made at room temperature within a volume of 0.9, 0.5, or 0.4  $\text{cm}^3$  for the WCu, WAl, or WI bead, respectively. All the data refinements dealing with the cell parameters and atomic positions were made by means of the Rietveld method and making use of the FullProf Suite program (LLB, CEA-Saclay, France).<sup>[46]</sup> The Thompson–Cox–Hastings pseudo-Voigt model fits well to the shape of the diffraction peaks of the phases. The intermetallic compounds located at or close to the faying interface in the WCu sample were characterized at a fine scale by TEM by means either of a Philips CM30 microscope (Philips, Amsterdam, the Netherlands) operating at 300 kV or of a 200 kV FEI Tecnai G2 20 apparatus (FEI Company, Hillsboro, OR). Both systems were equipped with precession electron diffraction and EDX devices. Thin foils were prepared by the focused ionic dual-beam (FIB) technique and using an FEI STRATA DB 325 microscope. They were located at the joint interface and at a depth of 670 (zone 1) or 1500  $\mu\text{m}$  (zone 2) from the top surface of the WCu weld (Figure 1). During cutting, the thin foil edge facing the ion beam was protected by a 2- $\mu\text{m}$ -thick deposit of platinum–tungsten. Electron backscattered diffraction (EBSD) analyses were also carried out in the vicinity of the WCu joint. A Bruker Nano high-resolution *e*Flash HR™ EBSD detector (Bruker AXS Inc., Madison, WI) mounted on a Zeiss Supra 55VP field-emission gun scanning electron microscopy (FEG SEM; Carl Zeiss, Oberkochen, Germany) was used.

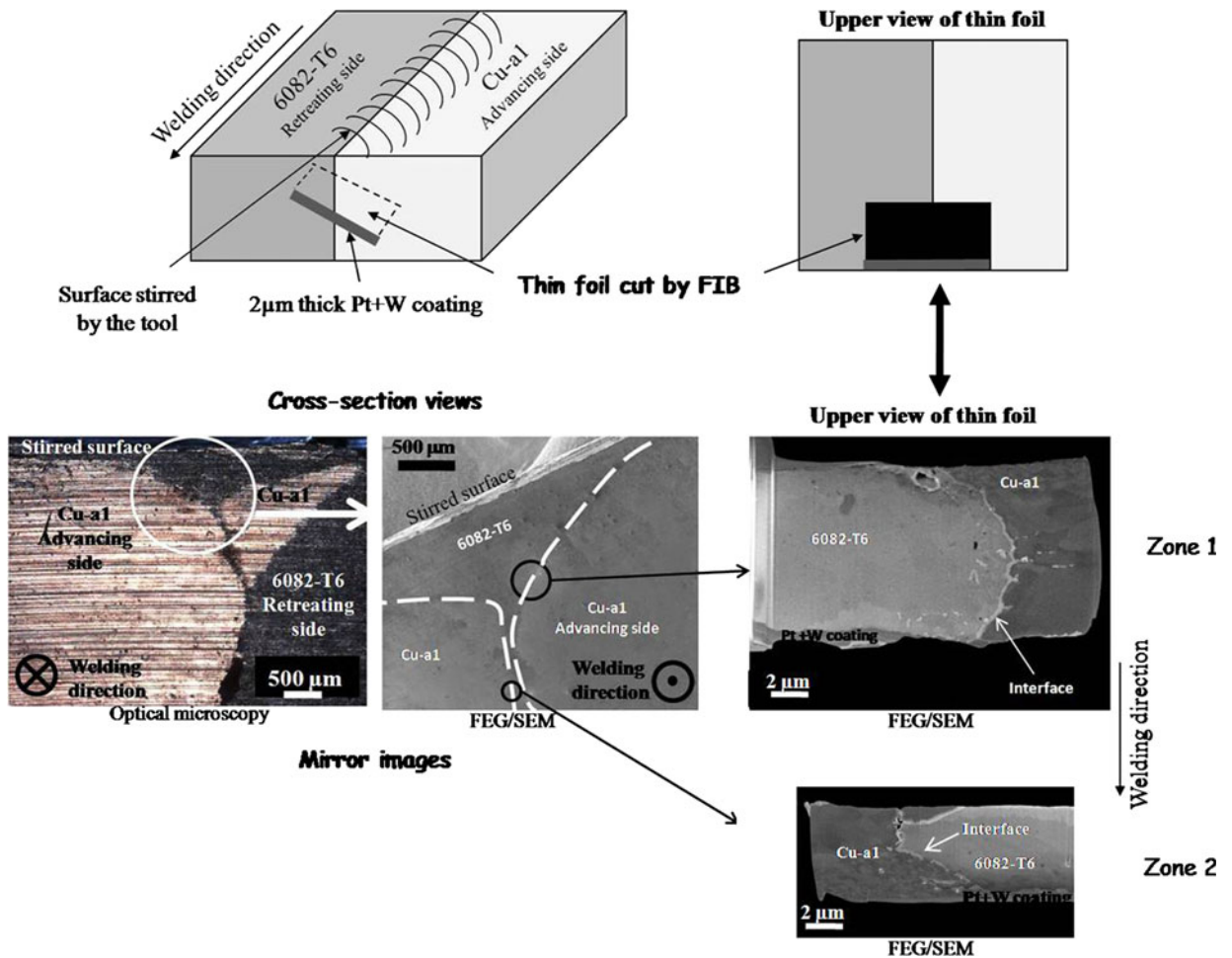


Fig. 1—Location of the thin foils cut by FIB at the FSW interface between Cu-a1 and 6082-T6 aluminum alloy.

### III. RESULTS AND DISCUSSION

As detailed in previous papers,<sup>[47,48]</sup> the malleability of Cu is insufficient for a suitable mechanical stirring, which requires an homologous temperature close to 0.8.<sup>[49]</sup> Indeed, according to the high thermal conductivity of both materials on the one hand, and to a well established expression of the peak temperature for Al alloys as a function of the rotation rate and of the travel speed of the tool on the other hand, welding is actually expected to proceed at a close to 723 K (450 °C) peak temperature,<sup>[50]</sup> and thus at a close to 0.75 and to 0.5 homologous temperature for the 6082 alloy and for the Cu base material, respectively.<sup>[47]</sup> In agreement with this insufficient malleability, determination of fracture initiation sites in the welds by means of both SEM and digital image correlation during tensile tests has proved that the most harmful flaw is a lack of consolidation.<sup>[48]</sup> Due to this deficient adhesion, the resulting mechanical properties were rather poor. For instance, the yield strength of the WCu joint amounts to 71 pct and 75 pct of that of the Al alloy and Cu base materials in the transverse direction, respectively. In accordance with this incomplete consolidation this joint efficiency markedly decreases with plastic deformation. The ultimate tensile strength indeed corresponds to only 49 pct and

58 pct of those of the Al alloy and Cu base materials, respectively. Besides this lack of consolidation, the deleterious effect of the softened zone on the Al side as well as the fracture of the intermetallic compounds (Figure 2) are at most of secondary importance for the mechanical behavior.

In spite of this result, the study of the nature and causes of formation of the present interfacial intermetallic compounds remains of the uppermost importance because of the promises of FSW with respect to the challenge imposed by dissimilar welding.

#### A. Macroscopic Analysis of the Joint

This section deals with the effect of the tool offset on the material flow with its consequences on the IMCs volume fraction.

Figure 3 shows the refinements of neutron diffraction patterns of the three kinds of welds. Irrespective of the tool location, only two intermetallic compounds, namely  $\gamma_1$ -Al<sub>4</sub>Cu<sub>9</sub> and  $\theta$ -Al<sub>2</sub>Cu, were detected. However, it is worthy to note that contrarily to the Al<sub>2</sub>Cu case, it remains difficult to resolve the diffraction peaks of the Al<sub>4</sub>Cu<sub>9</sub> phase. This problem is probably caused by the submicrometric grain size of Al<sub>4</sub>Cu<sub>9</sub>, which has been clearly proven (Figures 4 through 6). Furthermore,

concerning the estimation of the volume fraction of each IMC constituent, the processing of the neutron diffraction data was ticklish because of the small number of

peaks attributed to each compound (Figure 3). Nevertheless, Table I displays the IMCs volume fractions assessed by this procedure.

Table I shows that the IMC volume fraction differs according to the position of the tool. When the tool is offset from the interface, the amount of intermetallics is almost twofold the WI one. These differences are generated by the complex interaction of various parameters,

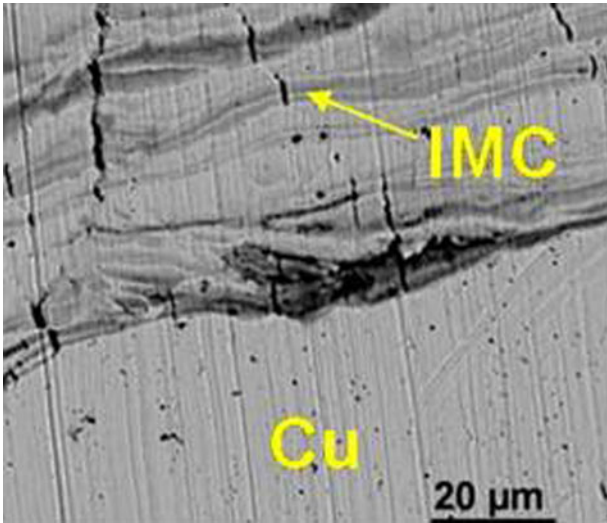


Fig. 2—Fractured intermetallic compounds observed on the surface of a polished tensile test sample (back scattered electrons [BSE]/SEM).

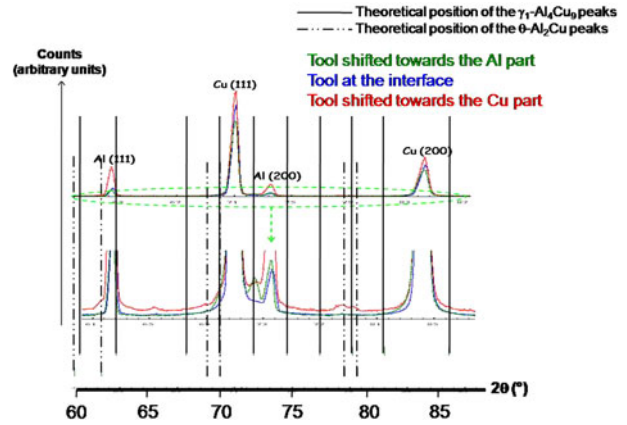


Fig. 3—Refined neutron diffraction pattern for each joint (These colored spectra are clearly differentiated in the electronic version of the paper).

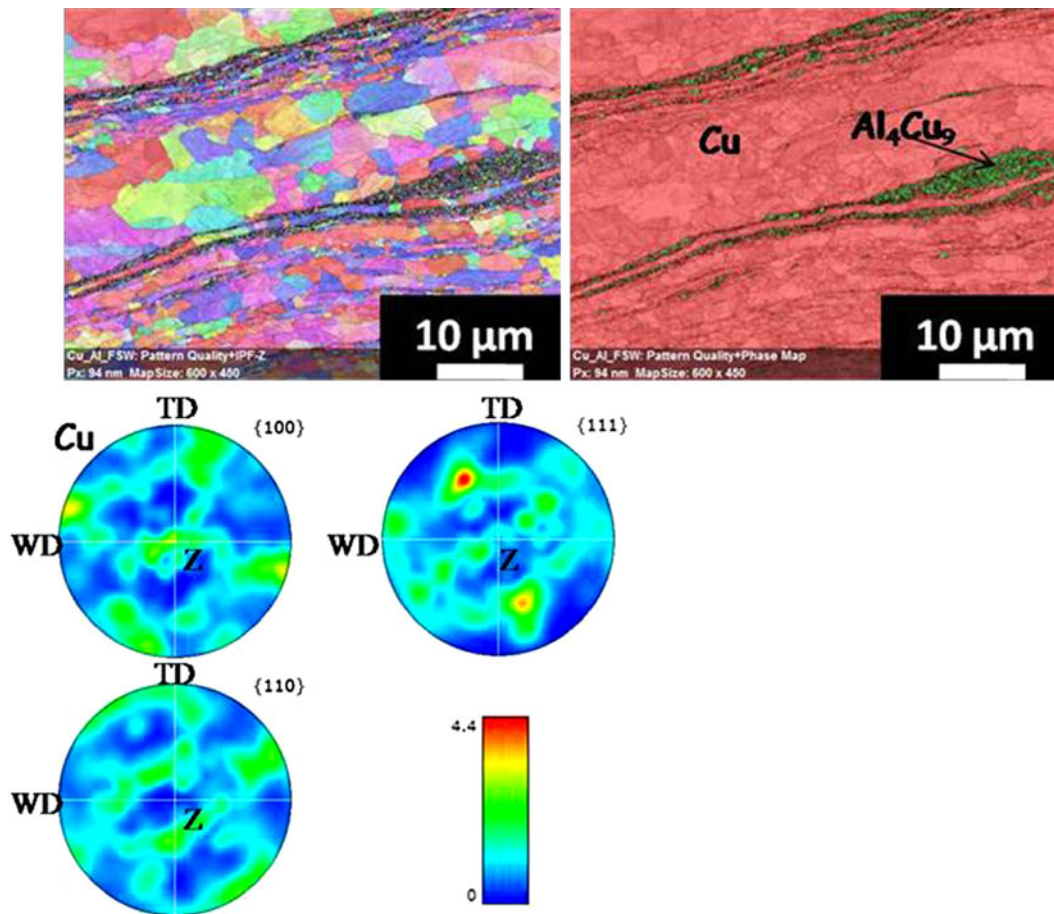


Fig. 4—Orientation images (EBSD) and Cu pole figures of zone A in Fig. 9 (WD, TD, and Z are the welding, transverse, and plate thickness directions, respectively). (Color figure online).

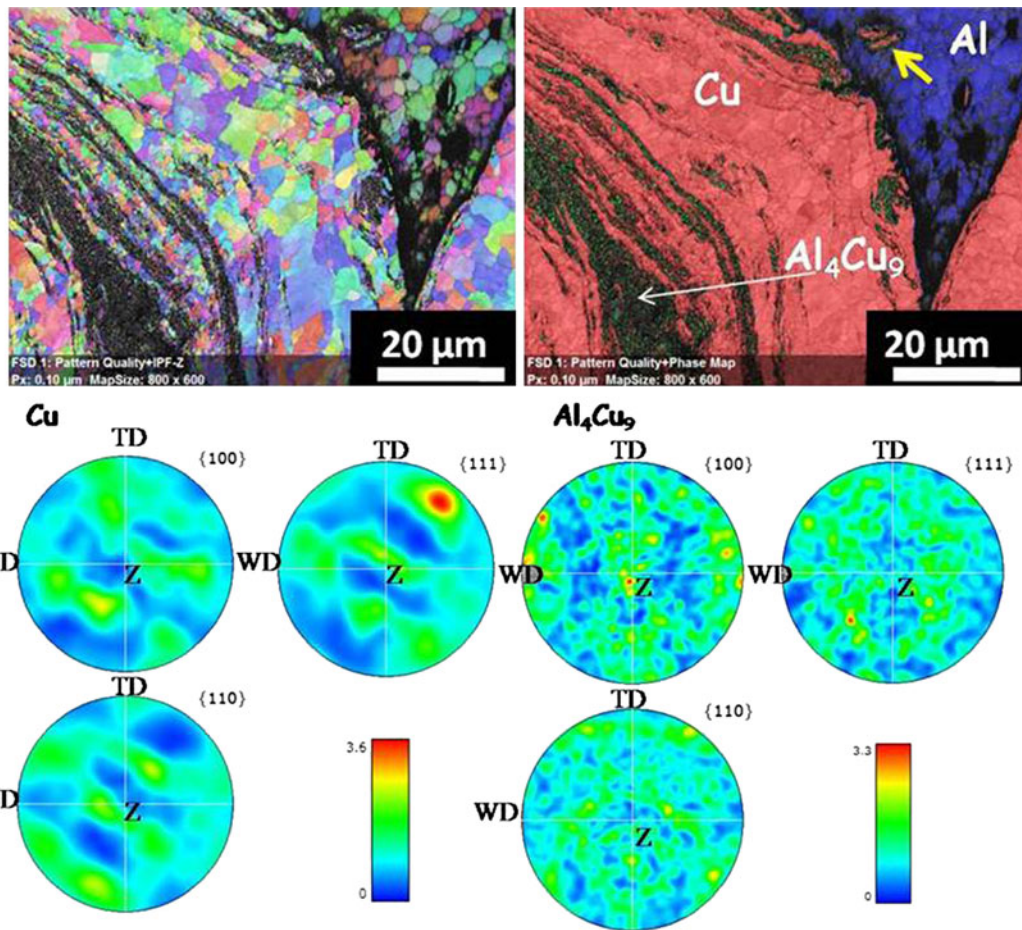


Fig. 5—Orientation images (EBSD) and Cu and  $\text{Al}_4\text{Cu}_9$  pole figures of zone B in Fig. 9 (WD, TD, and Z are defined in Fig. 4 caption). (Color figure online).

that is to say, the heat input, the temperature field, and the ease of plastic flow, which governs the distribution of both the amplitude and rate of plastic strains, and therefore, the local mixing between the components. As explained in the introduction, all of these variables are indeed expected to govern the IMC nature as well as their kinetics of formation. The heat generated by metalworking will increase with the resistance of the base material to deform. In the present case, the less malleable component of the bead is Cu because of its low homologous temperature and its higher flow stress at welding temperature.<sup>[21]</sup> In addition, the volume fraction of Cu in the stir zone directly depends on the tool location with respect to the faying interface. Therefore, this amount of Cu as well as the ensuing heat input increases in the order WAl, WI, and WCu. In case of dissimilar Al-Cu FSW, an augmentation of peak temperature by some decades has indeed been observed on the side of the Cu stronger alloy.<sup>[51]</sup> In accordance with this argumentation and, therefore, with the kinetics of thermal diffusion of Al and Cu, the WCu sample contains the highest volume fraction of IMCs. This temperature effect is, however, in contradiction with the higher amount of IMCs in WAl than in WI. The  $\text{Al}_4\text{Cu}_9$ , and therefore the Cu-rich chemical composition of the predominant IMC found in WAl, is further inconsistent

with both the primitive availability in solute and the far higher thermal mobility of Cu in Al than of Al in Cu.<sup>[52,53]</sup> In fact, at the 773 K (500 °C) expected peak temperature the coefficient of interdiffusion actually ranges from 5.8 to  $1.5 \times 10^{-10} \text{ cm}^2 \cdot \text{s}^{-1}$  in presence of 3.05 at. pct of Cu against only  $1.7 \times 10^{-12} \text{ cm}^2 \cdot \text{s}^{-1}$  in Cu-15 at. pct Al to Cu-20.7 at. pct Al alloys.<sup>[52]</sup> In addition, and again close to the actual peak temperature, the impurity diffusion coefficient of Cu in Al is four orders of magnitude higher than that of Al in Cu.<sup>[53]</sup> Moreover, the intrinsic diffusivity of Cu is again somewhat higher than that of Al in a thin film of  $\text{Al}_4\text{Cu}_9$ .<sup>[54]</sup> The latter proof is, however, more or less suitable according to several parameters such as the effects of the IMC layer thickness and of the elaboration process on the density of lattice defects within the IMC layer, and/or a possible change of the diffusion mechanism over the range of temperature extrapolation and/or the influence of the nature of the adjoining phases on the overall kinetics of atom displacement.

The complementary role of mechanical mixing must be taken into account in order to explain the WAl results. It is indeed relevant to note that the formation of an intermetallic compound relies on the apparition of local mixtures of atoms with a suitable chemical composition.<sup>[55,56]</sup> In addition, a sharp concentration

**Table I. Volume Fractions of IMCs within the Welds\***

Phases (vol pct)	WAl	WI	WCu
Al <sub>4</sub> Cu <sub>9</sub>	2.6	2.2	3.6
Al <sub>2</sub> Cu	1.4	0.2	1.7

\*The precision of these measurements is at least of 0.1 pct.

the case of the WCu sample as it contains the highest content in intermetallic compounds (Table I). This section essentially deals with the IMCs nature according to their location and kinetics of formation. It finally establishes their accelerated formation by FSW.

As mentioned in Section II, the metallurgical and chemical features of the bonding between the 6082 alloy and Cu-a1 were investigated in zones 1 and 2 (Figure 1), and therefore, at two depths from the top surface of the weld. The comparison of both areas put into evidence less well-defined subgrains boundaries within Cu in zone 2 than in zone 1. This observation arises from the difference of thermo-mechanical history of each zone according to its location within the weld. According to their magnitude, the misorientations measured by EBSD have for instance proved that either dynamic recrystallization or dynamic recovery has occurred from place to place (Figures 4 and 5). This result has further been checked by the comparison between the pole figures of the base metals and of the weld.<sup>[59]</sup> In addition, both the substructure of the dislocations boundaries and the invariable contrast of the dislocations cells indicate that the two materials have experienced dynamic recovery in zone 2 (Figure 7).

Due to the difference in malleability and, therefore, of plastic flow pattern of both parent materials, large debris of copper have penetrated inside the aluminum part of the weld.<sup>[47]</sup> Such a feature may give rise to the formation of IMCs particles in their place (shown by the white arrows in Figure 8). These large plate-shaped precipitates, with a length of approximately 500 nm and a width of approximately 200 nm, act as pinning centers for the Al alloy grain boundaries. In accordance with the global availability of atomic species, the electron diffraction patterns obtained with the precession mode are consistent with their Al<sub>2</sub>Cu nature. In other areas, EBSD further shows that small  $\gamma_1$ -Al<sub>4</sub>Cu<sub>9</sub> crystals were formed in close contact with some other massive debris of Cu (as shown by bold arrow in Figure 5).

### 1. Interpenetration bands

In the Cu side, stripes of primitive Al have penetrated into pure Cu over distances up to a few micrometers. These bands are marked by arrows on the left-hand side in Figure 6. They are made of nanograins with a size between 50 and 100 nm. Electron diffraction analyses prove that their P43m group space and their crystal lattice agree with the  $\gamma_1$ -Al<sub>4</sub>Cu<sub>9</sub> ones. These results are consistent with the issues of the EBSD/SEM analyses of similar zones (Figures 4 and 5), which are typical of the joint in the Cu side and close to the crown (Figure 9). As depicted by the pole figures in Figure 5, this  $\gamma_1$ -Al<sub>4</sub>Cu<sub>9</sub> phase presents a quasi-random texture that contrasts with the dominant [111] fiber texture due to the shear

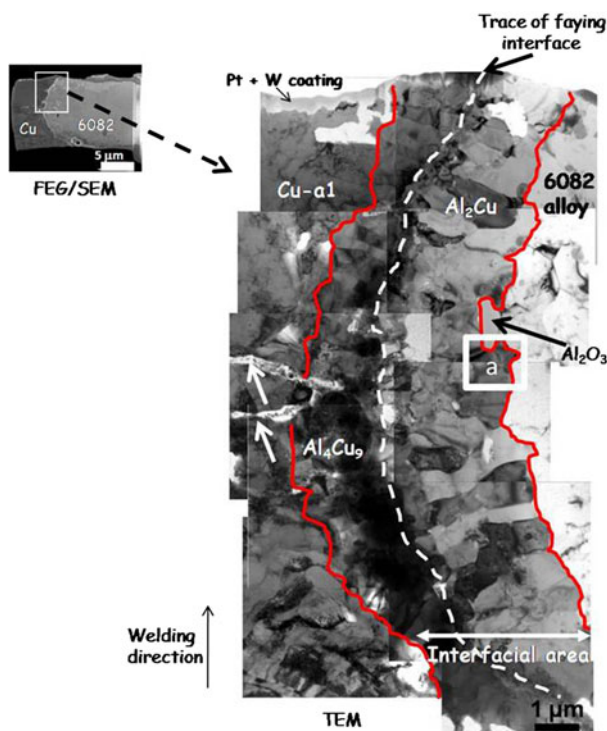


Fig. 6—Overall microstructure of the joint interface in zone 1 (TEM). Red lines (dark in a gray micrograph) delineate the boundaries of the IMC layer.

gradient inhibits the intermetallics nucleation.<sup>[57]</sup> Concerning the WAl sample and compared with its two other locations, the tool has to displace the lowest volume fraction of the Cu more resistant base material. The material flow is accordingly easier which by enhancing the mechanical stir of both materials is likely to generate more IMCs than in the WI joint in spite of a somewhat lower temperature. It should be noticed that this latter explanation agrees well with the presence of an incipient onion ring structure in the WAl joint which contrasts with the sharpness of the WI interface.<sup>[47]</sup> In accordance with the occurrence of a “forced” plastic deformation, the WCu sample further exhibits the most well-defined onion ring structure encountered in this study. It can be inferred from all of these results that by comparison with the cases of a predominant volume fraction of one component, mechanical mixing as well as material flow are significantly hampered during the metalworking of bulk bi-materials made of equivalent volume fractions of ductile components with distinct malleability. It is relevant to note that this remark agrees with the salient decrease of the fineness of mixing of the components with a diminution of the tool offset in the case of steel/Al friction-stirred welds.<sup>[58]</sup>

Besides, the Al<sub>4</sub>Cu<sub>9</sub> most frequent chemical composition of the reaction product for any tool offset is going to be discussed in the following.

### B. Local Analysis of the WCu Weld

The study of the microstructure of the welds at the finer scales of SEM/EBSD and TEM is only reported for

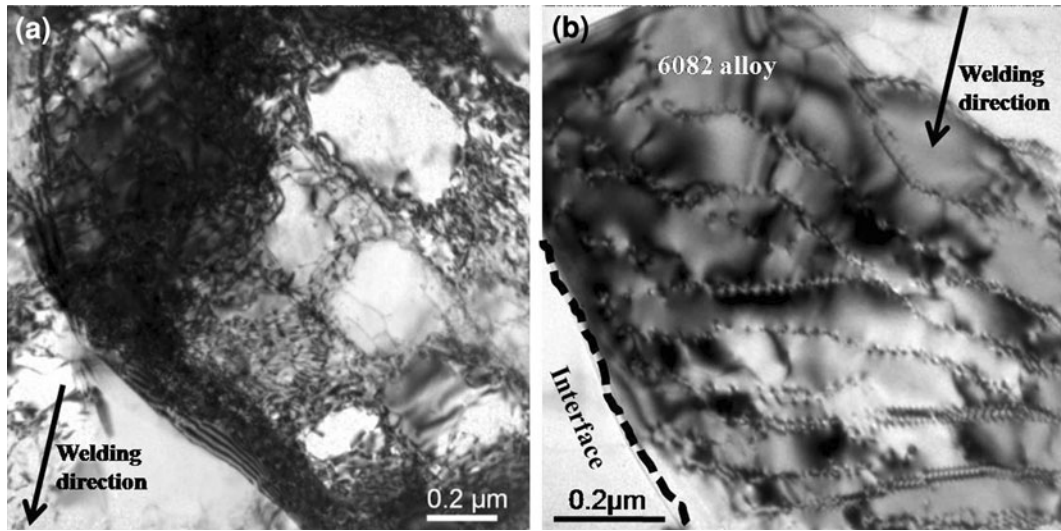


Fig. 7—TEM micrographs on either side and in close proximity of the interfacial IMC layer in zone 2: (a) Cu side and (b) 6082 alloy side.

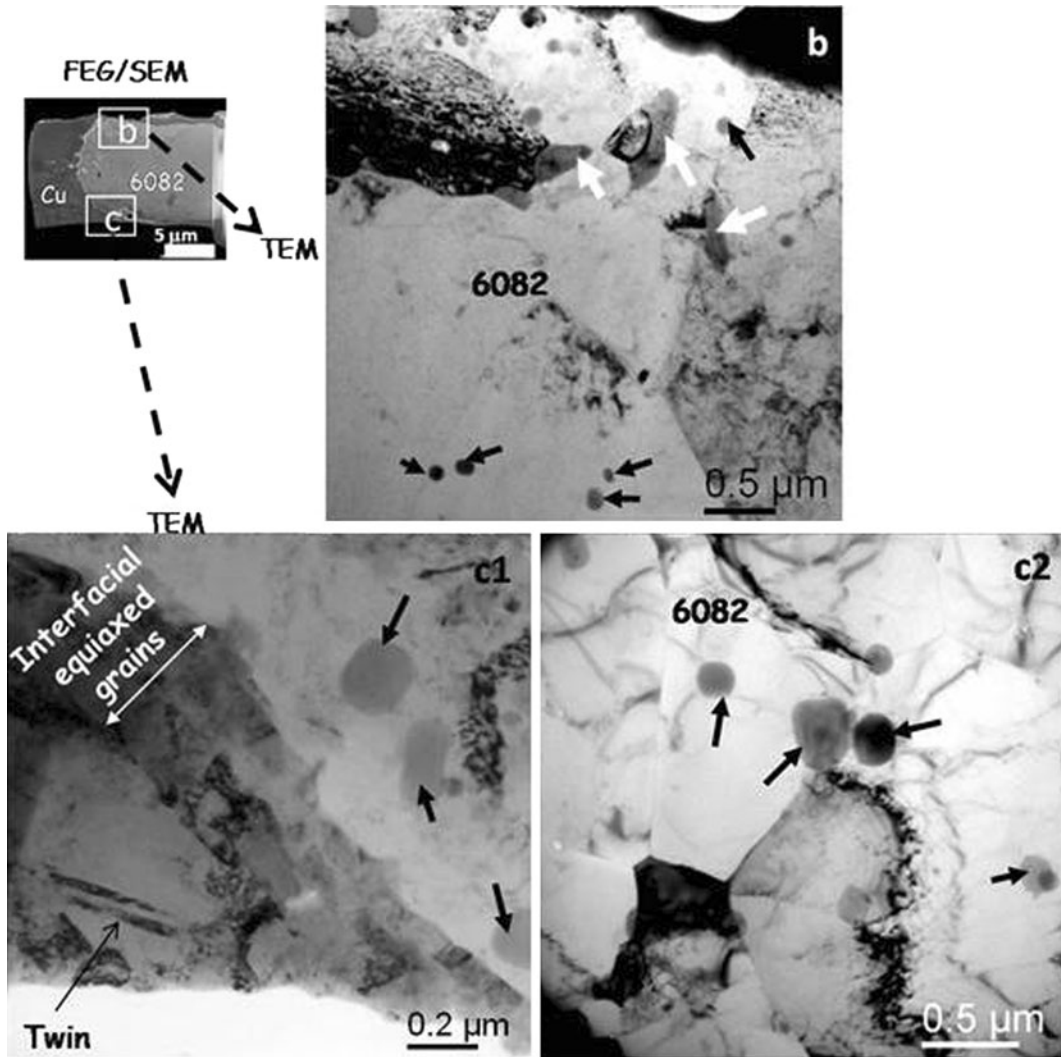


Fig. 8—Precipitation state in zone 1 (TEM): particles of  $\text{Al}_2\text{Cu}$  (white arrows) and of  $\text{Al}(\text{Fe},\text{Mn},\text{Cu})\text{Si}$  (black arrows).

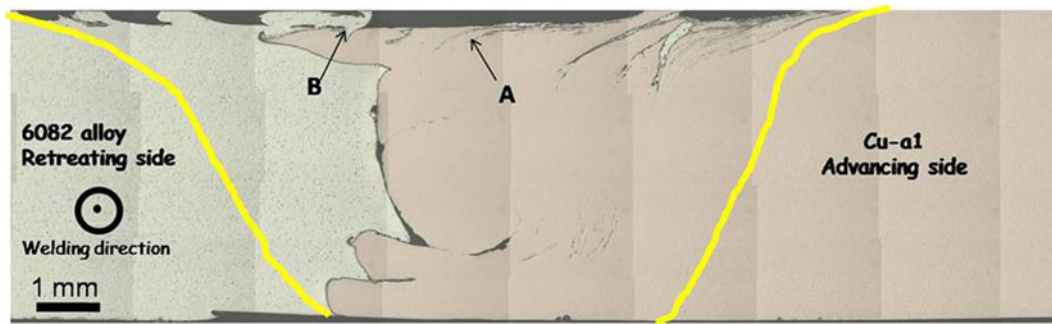


Fig. 9—Optical micrograph of the cross section of the WCu joint showing the limits of the nugget (yellow or white lines in the electronic version or in a gray picture, respectively).

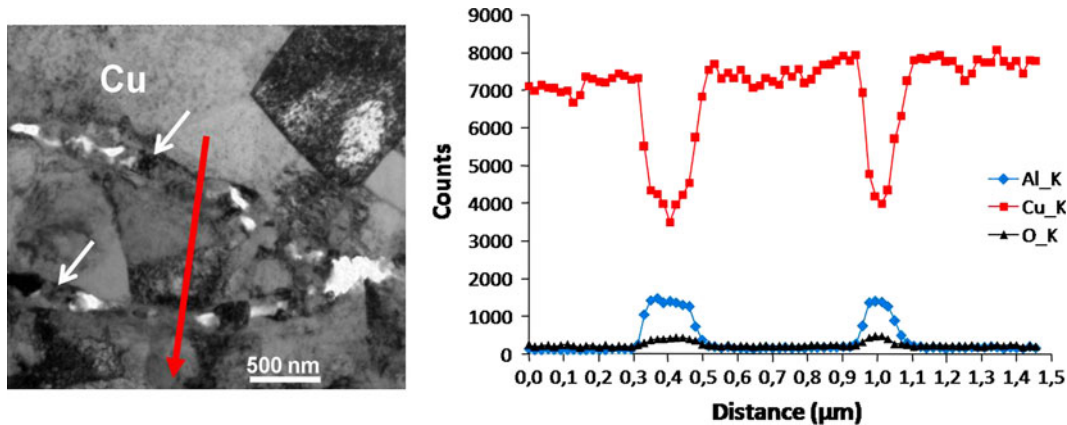


Fig. 10—Profiles of EDX analysis along the direction of the red arrow marked in the micrograph. This line, which appears in black in a grey micrograph, crosses two interpenetration bands (indicated by white arrows) in the Cu part.

deformation of Cu. Despite the primitive Al-rich chemical composition in the shear bands as well as the faster kinetics of diffusion of Cu in Al than the reverse,<sup>[52]</sup> and the comparison of the thermodynamical driving forces for precipitation of the various  $Al_xCu_y$  equilibrium IMCs (see the predictions of the effective heat of formation model in Section III-B-3),  $Al_4Cu_9$  forms preferentially to the  $Al_2Cu$  compound in these bands. In this regard, it seems worthy to note that this preferential reaction is assisted by both the relaxation of local residual stresses and the IMCs solubility range. The formation of  $\gamma_1-Al_4Cu_9$  indeed generates a volume contraction of approximately 23 pct against 10 pct for the  $\theta-Al_2Cu$  case. It is, therefore, more suitable in order to reduce the magnitude of the residual compressive stresses in the Al bands, which have deformed more easily than their surrounding Cu slugs. Besides, it has also been stated that the kinetics of growth of an intermetallic compound increase with its composition range and that this effect is as efficient as that of the coefficient of diffusion within this IMC.<sup>[60]</sup> According to the Al/Cu binary equilibrium phase diagram,<sup>[61]</sup> such an effect can, therefore, explain the higher kinetics of growth of  $\gamma_1-Al_4Cu_9$  compared with the  $\theta-Al_2Cu$  one.

EDX analyses have further established that the  $Al_4Cu_9$  intermetallic compounds are rich in oxygen (Figure 10) and sometimes in silicon and magnesium. The two latter elements very likely originate from the

dissolution during friction-stir welding of the  $Mg_2Si$  precipitates originally contained in the 6082-T6 aluminum alloy.<sup>[62–66]</sup>

## 2. Interface

Concerning the surface of contact between both metals, Figure 6 shows that it can be 3- to 4  $\mu m$  thick and composed of dislocation-free grains. A gradient of chemical composition is in particular noted across this interface. According to EDX profiles (not supplied in this article), which are displaying two plateaus, the interface comprises two kinds of  $Al_xCu_y$  compounds: an Al-rich and a Cu-rich intermetallic layer located on the Al alloy and on the Cu side, respectively. Both intermetallic layers display a thin sublayer of equiaxed nanograins with an average diameter of 300 nm at the faying surface. This central sublayer is prolonged by columnar grains that are perpendicular to the interface. In apparent contradiction with the predominant  $Al_4Cu_9$  volume fraction assessed by the neutron diffraction analyses of the bulk samples (Table I), Figure 6 depicts IMC basaltic grains that are more developed on the Al side. They are approximately 1  $\mu m$  long by 0.5  $\mu m$  wide against 0.5  $\mu m$  in length and 0.25  $\mu m$  in width on the Cu side. This discrepancy between the results of neutron diffraction and TEM analyses is expected to arise from both the miscellaneous nature of the thermomechanical history in FSW welds and the large difference of volume



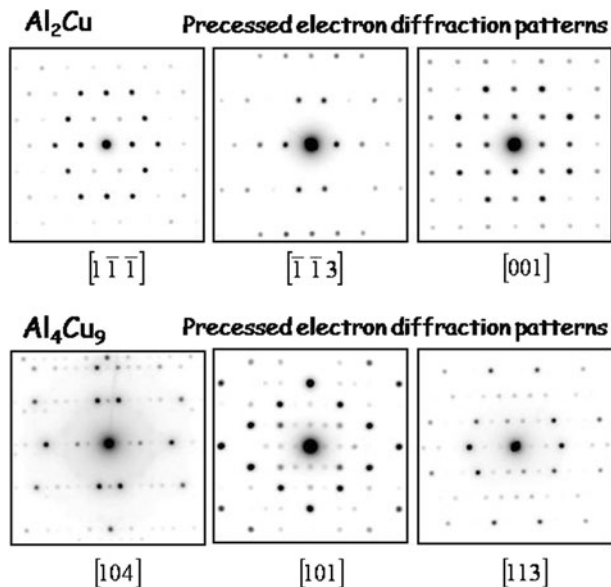


Fig. 11—Experimental precessed electron diffraction patterns of the  $\text{Al}_2\text{Cu}$  and  $\text{Al}_4\text{Cu}_9$  phases.

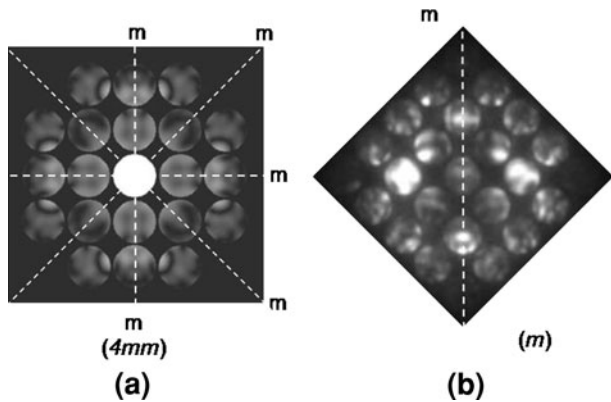


Fig. 12—(a) Theoretical [001] ZOLZ CBED pattern of the  $\text{Al}_2\text{Cu}$  phase showing the (4 mm) symmetry. (b) (m) symmetry of the experimental [001] ZOLZ CBED pattern recorded in the Al-rich side. The contrasts visible inside the diffracted disks result from the thickness variations, but they cannot affect the symmetry.

investigated with each technique. EDX spectroscopy combined with precessed electron diffraction analyses proves the presence of  $\text{Al}_4\text{Cu}_9$  and of  $\text{Al}_2\text{Cu}$  on the Cu and the 6082 side, respectively (Figure 11). Nevertheless, more accurate convergent beam electron diffraction (CBED) analyses showed that  $\text{Al}_2\text{Cu}$  possesses an unusual symmetry (Figure 12). The thermodynamically stable  $\theta\text{-Al}_2\text{Cu}$  phase has the tetragonal structure (I4/mcm, No. 140). Theoretically, and as shown in Figure 12(a), the highest “ideal” symmetry (*i.e.*, the symmetry taking into account the position and the diffracted intensity of each reflection on a zone axis pattern [ZAP]) of this phase should be (4 mm) on the [001] zero-order Laue zone (ZOLZ) ZAP obtained by CBED. By way of contrast, the experimental CBED pattern, displayed in Figure 12(b), only indicates the (m) symmetry. This decrease of symmetry discloses that the

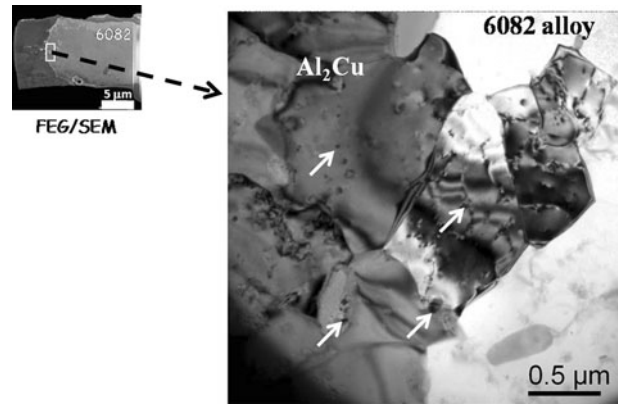


Fig. 13— $\text{Al}(\text{Fe},\text{Mn},\text{Cu})\text{Si}$  precipitates (marked by white arrows) into  $\text{Al}_2\text{Cu}$  IMCs (details of zone a in Fig. 6) (TEM).

formed phase does not correspond to usual  $\theta\text{-Al}_2\text{Cu}$ . Further details on this new phase will be addressed later in another article. This compound of unusual crystallography will be called “modified  $\text{Al}_2\text{Cu}$ .” Moreover, it is also worthy to note that rather large  $\text{Al}(\text{Fe},\text{Mn},\text{Cu})\text{Si}$  precipitates with both an equiaxed morphology and a mean diameter of approximately 20 nm are observed inside the columnar grains of modified  $\text{Al}_2\text{Cu}$  (Figure 13). This feature proves that these columnar grains have formed within the Al alloy side as  $\text{Al}(\text{Fe},\text{Mn},\text{Cu})\text{Si}$  precipitates are originating from the 6082-T6 alloy.<sup>[63]</sup> This observation is the most veracious as it has often been found that precipitates of this kind are not modified during the friction-stir welding of 6082-T6 alloys.<sup>[62–66]</sup> Not any microstructural evidence of an effect of these particles on the nucleation and growth of modified  $\text{Al}_2\text{Cu}$  has further been noticed.

Besides, the detection of very scarce and micrometer-sized alumina particles at the  $\text{Al}_2\text{Cu}/6082$  Al interface (Figure 6) very likely originates from the fracture during welding of an oxide layer present at the abutting interface of the Al plate before joining. This fragment was stuck into the surface of a slug of Al, which was machined during friction-stir welding. Such a fracture of an  $\text{Al}_2\text{O}_3$  layer entailed by a marked plastic deformation of its aluminum substrate has already been claimed to occur in other FSW studies.<sup>[67]</sup> In addition, and as illustrated by Figure 6, these large particles of alumina clearly hamper the growth of the  $\text{Al}_2\text{Cu}$  layer.

Figure 6 shows that, except the presence of the deep bands of penetration of Al on the Cu side, the interfaces are rather smooth between the IMCs layers and base materials. Such a feature suggests that the formation of these layers mainly occurs in the wake of the traveling tool.

To conclude on the current techniques of investigation of the microstructure, it seems worthy to emphasize that the TEM experiments have confirmed the neutron diffraction results while supplying further information on the IMCs nature and location in the weld. However, concerning the measurement of the IMCs volume fraction, it is worthy to emphasize that due to its too-fine scale of analysis, TEM generally leads to nonstatistical results, which may be misleading in

samples with a heterogeneous microstructure, as it is the case for FSW joints.

### 3. Nature of the intermetallic compounds

The formation of both  $\text{Al}_4\text{Cu}_9$  and modified  $\text{Al}_2\text{Cu}$  during friction-stir welding implies that welding was reactive. The observed stoichiometries are consistent with previous observations where the intermetallic phases at the interface were identified either by X-ray diffraction in an Al-Cu friction stirred weld<sup>[5,45,51]</sup> or by energy dispersive X-ray analysis (EDX/TEM) in an Al-Cu joint made by friction-stir diffusion.<sup>[68]</sup>

Such identifications of only two compounds may seem rather curious as the formation of six  $\text{Al}_x\text{Cu}_y$  equilibrium IMCs, *i.e.*,  $\theta$ - $\text{Al}_2\text{Cu}$ ,  $\eta_2$ - $\text{AlCu}$ ,  $\zeta_2$ - $\text{Al}_3\text{Cu}_4$ ,  $\delta$ ,  $\gamma_1$ - $\text{Al}_4\text{Cu}_9$ , and  $\alpha_2$ ,<sup>[61]</sup> and of a metastable one:  $\text{Al}_3\text{Cu}_2$ ,<sup>[69]</sup> is *a priori* possible with a close to 773 K (500 °C) peak temperature.

More strictly speaking, the modified  $\text{Al}_2\text{Cu}$ , identified for the first time in this study, has not been said to occur in the Al-Cu equilibrium phase diagram. So, due to this lack of thermodynamic data and at a first approximation, we are going to merge it with the usual  $\theta$ - $\text{Al}_2\text{Cu}$  phase. The formation of the  $\text{Al}_2\text{Cu}$  phase on the Al side of the weld is favored by both local chemical composition and thermodynamics. The very limited solubility of Cu in Al<sup>[61]</sup> explains the formation of the  $\text{Al}_2\text{Cu}$  phase, which is also the Al-richest phase among the  $\text{Al}_x\text{Cu}_y$  ones. This formation also agrees with the prediction of the effective heat of formation model according to which the first intermetallic phase to nucleate is the one with the most negative effective heat of formation at the composition of the lowest temperature of the liquidus.<sup>[70]</sup> In addition,  $\text{Al}_2\text{Cu}$  seems to be the first phase to nucleate at an Al-Cu interface by chemical interdiffusion.<sup>[71]</sup> The preferential growth of  $\text{Al}_2\text{Cu}$  displayed in Figure 6 is again consistent with the far higher diffusion rate of Cu in Al than of Al in Cu.<sup>[72]</sup> As a result, the growth rate of  $\text{Al}_2\text{Cu}$  is predominantly explained by the diffusion kinetics all the more as it presents a very narrow composition range. However, the exactness of this piece of reasoning dealing with diffusion remains questionable because of both the very likely difference of interface quality in various works and the rather unknown diffusion kinetics within intermetallics.

Due to the strain and stress conditions during the process, the existence of transitory IMCs, among which perhaps the modified  $\text{Al}_2\text{Cu}$  seems possible. The formation of out of equilibrium solid solutions pleads in favor of this suggestion.<sup>[73]</sup>

Concerning the nature of the IMC formed on the Cu side, it is relevant to note that it is not  $\alpha_2$ , *i.e.*, the Cu-richest compound among the  $\text{Al}_x\text{Cu}_y$  ones as should have been expected from the chemical composition of the base metal. In fact, the IMC formed on the Cu side is the  $\gamma_1$ - $\text{Al}_4\text{Cu}_9$  phase, which occupies the second rank among the Cu-rich compounds that can precipitate. Its formation occurs in spite of the predictions of the effective heat of formation model according to which  $\eta_2$ - $\text{AlCu}$  phase should be the second compound to precipitate.<sup>[70]</sup> However,  $\eta_2$ - $\text{AlCu}$  as well as the equilibrium  $\zeta_2$ - $\text{Al}_3\text{Cu}_4$  phases, which actually form during isothermal

treatments over the same temperature range,<sup>[11,74]</sup> were not observed at the faying interface. Compared with the  $\text{Al}_4\text{Cu}_9$  case, the formation of both  $\eta_2$ - $\text{AlCu}$  and  $\zeta_2$ - $\text{Al}_3\text{Cu}_4$  is expected to be hampered by their higher Al content. Always in comparison with  $\text{Al}_4\text{Cu}_9$ , the kinetics of growth of  $\alpha_2$ ,  $\eta_2$ , and  $\zeta_2$  are further assumed to be impaired by a limited composition range.<sup>[60]</sup> It must, however, be noted that in another Al-Cu friction-stirred weld, the  $\eta_2$ - $\text{AlCu}$  phase was found as isolated particles near the bottom of the stirred zone.<sup>[5]</sup> This clue suggests that the nature of the IMCs formed by reactive solid-state FSW is governed by both the local short thermal cycle (a few seconds) and the local chemical composition. These two main causes may also be assisted by the severe deformation amplitude and local internal stresses.<sup>[75]</sup>

### 4. Kinetics of formation of the intermetallic compounds

The kinetics of intermetallic formation seems to be exacerbated by friction-stir welding. Actually, with annealing conditions equivalent to the current FSW thermal history, *i.e.*, approximately 673 K (400 °C) for 10 seconds, a negligible thickness of intermetallic forms in cold-rolled bonded Al/Cu bimetallic plate.<sup>[11]</sup> Such an enhancement of kinetics due to FSW can also be inferred from the comparison with diffusion data obtained with defect-free interfaces according to which the diffusion length of Cu in Al is an order of magnitude smaller than the measured intermetallic thickness. The current assertion is again reinforced by the slower kinetics of diffusion in  $\text{Al}_x\text{Cu}_y$  compounds.<sup>[54]</sup> Such an acceleration of the kinetics of diffusion is the most significant as the interface must not be defect free in FSW-processed samples. The increase of kinetics of IMCs formation by FSW arises from the material flow that brings about mechanical mixing, short circuit diffusion, and a high supersaturation of vacancies.<sup>[3,4,27–32,35,39]</sup> In support of this settlement, the efficiency of defect-induced atomic diffusion on the kinetics of IMC formation during Al/steel friction-stir spot welding (FSSW) has been recently established from the comparison with results obtained with solid-state diffusion couples.<sup>[76]</sup> The latter deduction is the most relevant as, due to a significant gap between the tip of the probe and the faying interface, the FSSW plastic flow has occurred only within the upper plate of aluminum and without any deformation of the joint interface.

## IV. CONCLUSIONS

The main conclusions of the present paper are summarized as follows:

1.  $\text{Al}_2\text{Cu}$  and  $\gamma_1$ - $\text{Al}_4\text{Cu}_9$  phases are formed in dissimilar Al 6082-T6/Cu friction-stir weld under the used conditions. Their formation is essentially governed by both the thermomechanical history and the local mixing of the chemical species.
2. The  $\text{Al}_2\text{Cu}$  compound is termed “modified” as it possesses an unusual crystal symmetry. This, heretofore, unknown symmetry suggests its out of equilibrium conditions of formation.

3. The volume fraction of both  $\gamma_1$ -Al<sub>4</sub>Cu<sub>9</sub> and modified Al<sub>2</sub>Cu depends on the tool offset because of the predominant effect of the material flow pattern.
4. The rather thick interface of the joint is composed of equiaxed and columnar grains of both kinds of intermetallics.

## ACKNOWLEDGMENTS

Many thanks are due to the IS French Welding Institute for providing the samples, to G. André (LLB, Saclay) for neutron diffraction experiments, and to Dr. D. Troadec (IEMN, Villeneuve d'Ascq) for preparing FIB specimens. The TEM facility in Lille (France) is supported by the Conseil Regional du Nord-Pas de Calais and the European Regional Development Fund (ERDF).

## REFERENCES

1. P.L. Threadgill, A.J. Leonard, H.R. Shercliff, and P.J. Withers: *Int. Mater. Rev.*, 2009, vol. 54, pp. 49–93.
2. M. Ericsson and R. Sandström: *Int. J. Fatigue*, 2003, vol. 25, pp. 1379–87.
3. R.S. Mishra and Z.Y. Ma: *Mater. Sci. Eng. R*, 2005, vol. 50, pp. 1–78.
4. R. Nandan, T. DebRoy, and H.K.D.H. Bhadeshia: *Progr. Mater. Sci.*, 2008, vol. 53, pp. 980–1023.
5. P. Xue, B.L. Xiao, D.R. Ni, and Z.Y. Ma: *Mater. Sci. Eng. A*, 2010, vol. 527, pp. 5723–27.
6. T. Laurida, V. Vuorinen, and J.K. Kivilahti: *Mater. Sci. Eng. R*, 2005, vol. 49, pp. 1–60.
7. M. Braunovic and M. Alexandrov: *IEEE Trans. Compon. Packag. Manuf. Technol., Part A*, 1997, vol. 17, pp. 78–85.
8. H.J. Park, S. Rhee, M.J. Kang, and D.C. Kim: *Mater. T. JIM*, 2009, vol. 50, pp. 2314–17.
9. M. Abbasi, A.K. Taheri, and M.T. Salehi: *J. Alloy. Compd.*, 2001, vol. 319, pp. 233–41.
10. Y.J. Su, X.-H. Liu, H.-Y. Huang, X.-F. Liu, and H.-X. Xie: *Metall. Mater. Trans. A*, 2011, vol. 42A, pp. 4088–99.
11. C.-Y. Chen, H.-L. Chen, and W.-S. Hwang: *Mater. Trans. JIM*, 2006, vol. 47, pp. 1232–39.
12. M. Aonuma and K. Nakata: *Mater. Sci. Eng. B*, 2010, vol. 173, pp. 135–38.
13. A. Hirose, H. Imaeda, M. Kondo, and K.F. Kobayashi: *Mater. Sci. Forum*, 2007, vols. 539–543, pp. 3888–93.
14. T. Tanaka, T. Morishige, and T. Hirata: *Scripta Mater.*, 2009, vol. 61, pp. 756–59.
15. M. Aonuma and K. Nakata: *Mater. Sci. Eng. B*, 2010, vol. 173, pp. 135–38.
16. K. Savolainen, J. Mononen, T. Saukkonen, and H. Hänninen: *Proc. Int. Symp. FSW*, 2006, Paper 79.
17. K. Ueda, T. Ogura, S. Nishiuchi, K. Miyamoto, T. Nanbu, and A. Hirose: *Mater. T. JIM*, 2011, vol. 52, pp. 967–73.
18. D.-H. Choi, B.-W. Ahn, C.-Y. Lee, Y.-M. Yeon, K. Song, and S.-B. Jung: *Intermetallics*, 2011, vol. 19, pp. 125–30.
19. T. Ogura, K. Ueda, Y. Saito, and A. Hirose: *Mater. Trans. JIM*, 2011, vol. 52, pp. 979–84.
20. J. Wilden, J.P. Bergmann, and S. Jahn: *Adv. Eng. Mater.*, 2006, vol. 8, pp. 212–18.
21. Smithells Metal Reference Book, 7th ed., E.A. Brandes and G.B. Brook, eds., Oxford, U.K., 1992.
22. W. Zhou, L. Liu, B. Li, Q. Song, and P. Wu: *J. Electron. Mater.*, 2009, vol. 38 (2), pp. 356–64.
23. A.I. Zaitsev, N.E. Zaitseva, R.Y. Shinko, N.A. Arutyunyan, S.F. Dunaev, V.S. Kraposhin, and H.T. Lam: *J. Phys. Cond. Matter.*, 2008, vol. 20, pp. 114121.
24. M. Kowalski and P.J. Spencer: *J. Phase Equil.*, 1993, vol. 14 (4), pp. 432–38.
25. M. Watanabe, K. Feng, Y. Nakamura, and S. Kumai: *Mater. Trans. JIM*, 2011, vol. 52, pp. 953–59.
26. S. Takeshi, O. Masafumi, E. Seiichi, and M. Kazuya: *Q. J. Jpn. Weld. Soc.*, 2000, vol. 18, pp. 365–72.
27. A. Arora, Z. Zhang, A. De, and T. DebRoy: *Scripta Mater.*, 2009, vol. 61, pp. 863–66.
28. P. Heurtier, C. Desrayaud, and F. Montheillet: *Mater. Sci. Forum*, 2002, vols. 396–402, pp. 1537–42.
29. H. Schmidt and J. Hattel: *Modell. Simul. Mater. Sci. Eng.*, 2005, vol. 13, pp. 77–93.
30. G. Buffa, J. Hua, R. Shivpuri, and L. Fratini: *Mater. Sci. Eng. A.*, 2006, vol. 419, pp. 381–88.
31. G. Buffa, J. Hua, R. Shivpuri, and L. Fratini: *Mater. Sci. Eng. A.*, 2006, vol. 419, pp. 389–96.
32. K. Masaki, Y.S. Sato, M. Maeda, and H. Kokawa: *Scripta Mater.*, 2008, vol. 58, pp. 355–60.
33. M. Militzer, W.P. Sun, and J.J. Jonas: *Acta Metall. Mater.*, 1994, vol. 42, pp. 133–41.
34. I.E. Gunduz, T. Ando, E. Shattuck, P.Y. Wong, and C.C. Doumanitis: *Scripta Mater.*, 2005, vol. 52, pp. 939–43.
35. K.V. Jata and S.L. Semiatin: *Scripta Mater.*, 2000, vol. 43, pp. 743–49.
36. Ø. Frigaard, Ø. Grong, and O.T. Midling: *Metall. Mater. Trans. A*, 2001, vol. 32A, pp. 1189–1200.
37. A. Gerlich, G. Avramovic-Cingara, and T.H. North: *Metall. Mater. Trans. A*, 2006, vol. 37A, pp. 2773–86.
38. C.I. Chang, C.J. Lee, and J.C. Huang: *Scripta Mater.*, 2004, vol. 51, pp. 509–14.
39. A. Askari, S. Silling, B. London, and M. Mahoney: *Friction Stir Welding and Processing*, TMS, Warrendale, PA, 2001, pp. 43–54.
40. R. Qiu, S. Satonaka, and C. Iwamoto: *Mater. Des.*, 2009, vol. 30, pp. 3686–89.
41. R. Ayer, H.W. Jin, R.R. Mueller, S. Ling, and S. Ford: *Scripta Mater.*, 2005, vol. 53, pp. 1383–87.
42. W.B. Lee, M. Schmuecker, U.A. Mercado, G. Biallas, and S.B. Jung: *Scripta Mater.*, 2006, vol. 55, pp. 355–58.
43. K.S. Bang, K.J. Lee, H.S. Bang, and H.S. Bang: *Mater. Trans.*, 2011, vol. 52 (5), pp. 974–78.
44. A. Kostka, R.S. Coelho, J. dos Santos, and A.R. Pyzalla: *Scripta Mater.*, 2009, vol. 60, pp. 953–56.
45. P. Xue, D.R. Ni, D. Wang, B.L. Xiao, and Z.Y. Ma: *Mater. Sci. Eng. A*, 2011, vol. 528, pp. 4683–89.
46. FullProf: WinPLOTR Software, A Graphic Tool For Powder Diffraction, Version 2006.
47. M.N. Avettand-Fènoël, R. Taillard, C. Herbelot, and A. Imad: *Mater. Sci. Forum*, 2010, vols. 638–642, pp. 1209–14.
48. M.-N. Avettand-Fènoël, R. Taillard, and G. Ji: *Mater. Sci. Forum*, 2012, vols. 706–709, pp. 959–64.
49. T.R. McNelley, S. Swaminathan, and J.Q. Su: *Scripta Mater.*, 2008, vol. 58, pp. 349–54.
50. S.R. Ren, Z.Y. Ma, and L.Q. Chen: *Scripta Mater.*, 2007, vol. 56, pp. 69–72.
51. H.J. Liu, J.J. Shen, L. Zhou, Y.Q. Zha, C. Liu, and L.Y. Kuang: *Sci. Technol. Weld. Joi.*, 2011, vol. 16 (1), pp. 92–98.
52. W. Jost: *Diffusion in Solids, Liquids, Gases*, E.M. Loebel, ed., Academic Press, New York, NY, 1960.
53. D. Liu, L. Zhang, Y. Du, H. Xu, S. Liu, and L. Liu: *CALPHAD*, 2009, vol. 33, pp. 761–68.
54. H.T.G. Hentzell and K.N. Tu: *J. Appl. Phys.*, 1983, vol. 54, pp. 6929–37.
55. R. Taillard, C.E. Bruzek, and E. Florianova: *Proc. Int. Conf. Solid to Solid Phase Transformations*, Nemacon Woodlands, PA, TMS, Warrendale, PA, 1994, pp. 1183–88.
56. D.Y. Ying and D.L. Zhang: *J. Alloy. Compd.*, 2000, vol. 311, pp. 275–82.
57. F. Hodaj and P.J. Desré: *Acta Mater.*, 1996, vol. 11, pp. 4485–90.
58. T. Watanabe, H. Takayama, and A. Yanagisawa: *J. Mater. Process. Technol.*, 2006, vol. 178, pp. 342–49.
59. D. Goran, G. Ji, M.N. Avettand-Fènoël, and R. Taillard: *Mater. Sci. Forum*, 2012, vols. 702–703, pp. 574–77.
60. M. Kajihara: *Acta Mater.*, 2004, vol. 52, pp. 1193–1200.
61. N. Ponweiser, C.L. Lengauer, and K.W. Richter: *Intermetallics*, 2011, vol. 19, pp. 1737–46.

62. R. Taillard, M.N. Avettand-Fènoël, C. Herbelot, and A. Imad: *Proc. Journées Annuelles de la Société Française de Métallurgie et de Matériaux*, Nancy, France, 2011.
63. A. Simar, Y. Bréchet, B. de Meester, A. Denquin, C. Gallais, and T. Pardoën: *Progr. Mater. Sci.*, 2012, vol. 57 (1), pp. 95–183.
64. L.E. Svensson, L. Karlsson, H. Larsson, B. Karlsson, M. Fazzini, and J. Karlsson: *Sci. Tech. Weld. Joi.*, 2000, vol. 5, pp. 285–96.
65. Y.S. Sato, M. Urata, and H. Kokawa: *Metall. Mater. Trans. A*, 2002, vol. 33A, pp. 625–35.
66. G. Mrówka-Nowotnik and J. Sieniawski: *J. Mater. Process. Technol.*, 2005, vols. 162–163, pp. 367–72.
67. T. Watanabe, A. Yoneda, A. Yanagisawa, S. Konuma, and O. Ohashi: *Yosetsu Gakkai Ronbunshu*, 1999, vol. 17, pp. 223–33.
68. M. Girard, B. Huneau, C. Genevois, X. Sauvage, and G. Racineux: *Sci. Tech. Weld. Joi.*, 2010, vol. 15, pp. 661–65.
69. P. Ramachandrarao and M. Laridjani: *J. Mater. Sci.*, 1974, vol. 9, pp. 434–37.
70. R. Pretorius, T.K. Marais, and C.C. Theron: *Mater. Sci. Eng. R*, 1993, vol. 10, pp. 1–83.
71. D. Moreno, J. Garrett, and J.D. Embury: *Intermetallics*, 1999, vol. 7, pp. 1001–09.
72. X.K. Peng, R. Wührer, G. Heness, and W.Y. Yeung: *J. Mater. Sci.*, 1999, vol. 34, pp. 2029–38.
73. L.E. Murr: *J. Mater. Eng. Perf.*, 2010.
74. Y. Funamizu and K. Watanabe: *Trans. Jpn. Inst. Met.*, 1971, vol. 12, pp. 147–52.
75. S. Guyot: Ph.D. Dissertation, University of Lille 1, France, 2005.
76. M. Watanabe, K. Feng, Y. Nakamura, and S. Kumai: *Mater. Trans.*, 2011, vol. 52, pp. 953–59.